Проведеними розрахунковими дослідженнями в моделі обойма-діелектрична матриця-верхній електрод-пуансон-спікаємий кільцевий виріб-нижній електрод-пуансон-підставка було визначено кінетику температурних змін. Завдяки цьому стало можливим визначення температури контрольних об'ємів виробу і оснастки в довільний проміжок часу. Експериментами підтверджено, що розрахункові значення температури в верхніх та нижніх шарах спікаємого виробу доволі подібні між собою і мало відрізняються від реальних. Зокрема встановлено, що в спікаємому виробі зосереджується 24 % теплової енергії, яке виділяється у всьому блоці (прес-інструмент-виріб). При кондукційному способі нагріву дуже важливо у самий короткий проміжок часу досягнути максимальної температури у зоні спікаємого виробу.

Показано, що при експлуатації матеріал прес-форми в умовах електроспікання піддається термоциклічному і термомеханічному впливу. Компоненти оснастки мають різну стійкість до зносу: ресурс ізольованої вставки складає 20 циклів спікання, електродів – пуансонів 50 циклів. Це дозволяє стверджувати, що необхідно підібрати матеріал складових прес-форми, який би відповідав наступним вимогам:

– мінімальний нагрів елементів оснастки, забезпечуючих її конструкційну надійність та експлуатаційну технологічність (обойма, матриця, підставка);

– максимальний нагрів ланцюжка: верхній електрод-пуансон-ігла-спікаємий виріб-нижній кільцевий електрод-пуансон, сприяючий акумулюванню тепла в зоні дотику ділянок компонентів прес-форми з майбутнім виробом.

Вищевказані заходи призводять до підвищення структурної міцності спечених виробів, а також оптимізації контролю майбутніх технологічних операцій та оперативної фіксації важливих експериментальних даних.

Таким чином, є підстави стверджувати про можливість спрямованого регулювання температурних полів шляхом попереднього розрахунку та вибору матеріалів оснастки по теплофізичним характеристикам. Використання даної математичної моделі є ефективним способом рішення вищевказаного питання

Ключові слова: метод контрольних об'ємів, прес-інструмент, тепловий поток, електроспікання, джоулів нагрів

UDC 669.01:621.048
DOI: 10.15587/1729-4061.2020.205500

STUDYING THE EFFECT OF ESTIMATED PARAMETERS ON THE DISTRIBUTION OF TEMPERATURE ZONES IN THE ELEMENTS OF A MOLD UNDER CONDITIONS OF ACTIVATED PROCESSING

A. Morozov
PhD, Associate Professor*
E-mail: morozov.and@ukr.net
V. Olijnyk
PhD, Associate Professor*
E-mail: Oleinik06@ukr.net
*Department of Printing Technology Institute of Publishing and Printing
National Technical University of Ukraine "Igor Sikorsky Kyiv Polytechnic Institute"
Peremohy ave., 37, Kyiv, Ukraine, 03056

Received date 20.04.2020
Accepted date 10.06.2020
Published date 30.06.2020

1. Introduction

In the process of electric discharge processing of metal powders and alloys on their basis, there is a simultaneous effect exerted on the material of the press-tool by electric current, high temperatures, and pressure. This significantly complicates the task of selecting materials without preliminary calculations, which would make it possible to establish the technological principles for creating more resistant combined tooling elements for electric sintering [1]. The research into the development of materials for the mold is important for the practice of technological processes in powder metallurgy. Electric sintering allows for the compatibility of pressing and sintering processes, thereby freeing the production areas taken up by the equipment.

Based on the developed model, one can derive the heat distribution in the parts of a press tool and in the sintered powder product. Choosing the optimum tooling material for electric sintering conditions greatly simplifies the mathematical modeling of the tooling heating process.

The numerical solution to the derived system of equations makes it possible to determine the temperature of the control volumes of the product and tooling in a random period. The calculations, similar to those described, allow the comparison of the progress of the activated process at various structural and material-science solutions for building a press-tool, as well as the quantification of the technical and economic evaluation of the entire technological link.

2. Literature review and problem statement

The use of modern methods of electrophysical treatment makes it possible to obtain materials with a new level of physical and mechanical properties, thus reducing the sintering temperature and aging time. The method of compacting of powdered products by electric sintering ensures the even distribution of density in the molds of complex shape without application of any plasticizers, which are the potential sources of impurities and additional porosity in would-be products [2]. The authors of papers [3, 4], to study the heating of porous materials, developed the methods for calculating a temperature distribution lengthwise the electrode-punches and a sintered product in contact with them. They considered a typical scheme to transmit electric current through a sample under the simplified assumption that there is no outflow of heat in the side directions. The specified methods provide an opportunity to derive formulae for one-dimensional temperature distribution in the resulting product and in the electrodes-punches in contact with it. More complex temperature fields occur at the electric sintering of annular products [5]. It is of great importance, in this case, to mathematically model those complex temperature transformations that take place in the contact area of different materials of the mold [6].

The electric sintering should be considered a new, quite promising way that enables the use of heat, which is released as a result of micro discharges, as well as joule heating. A given technique intensifies the processes of thermal, electrostatic, and ionic diffusion in the area of inter-partial contact, which ensures short-term sintering of powder mixtures yielding the high-strength products [7]. However, electric sintering, as a kind of hot pressing, is characterized not only by the intensive mass transfer between the mixtures' components but also between the powder particles and the molds' components. The result of the mass transfer is the processes of baking the powder (adhesion) to the electrodes-punches. In this connection, the task of the choice and development of materials for the press-tool is fundamental for the industrial implementation of this technique [8]. The main criterion for such materials is their resistance to sudden increases in temperature because, under the influence of electric current, their rapid heating occurs [9].

Paper [10] reports the results of studying the heating of porous materials with electric current; however, the heat and electrophysical processes in the electrodes-punches are disregarded. In work [11], an equation for the temperature in metal between the electrodes was derived taking into consideration the heat transfer in the electrodes; however, no expression for the temperature field in electrodes is provided. When using a finite element method for the calculation of the temperature of the powder through which the electric current is passed [12], the electrodes-punches are accepted to be homogeneous in space but do not coincide with each other. The above papers do not take into consideration the porosity of a treated sample, as well as the thermal- and electrophysical parameters and densities with the temperature.

The reason for this may be the objective difficulties, which are associated with the high cost of conducting experimental research: this is especially true of the hardware that registers many parameters in the activated processes. Such factors make it impractical to conduct the above studies.

A variant for overcoming such difficulties can be those works that address the mathematical modeling of thermal processes in the process of passing an electric current through the system electrode-punch-sample-electrode-punch [13]. This paper formulates an assumption about the absence of real conditions to divert the heat from the areas of the electrode-punch in contact with a sample.

In the theory of heating complex electrical conductors [14], the temperature fields, which would make it possible to take into consideration all thermophysical processes in a sample and the electrodes-punches in contact with it, were not calculated. Consequently, it is difficult to experimentally establish an accurate distribution of temperature in the press-tool elements, taking into consideration a different combination of their materials, which possess a wide enough range of thermophysical properties [15].

Therefore, there are reasons to believe that the lack of certainty in the influence of additional parameters, namely, technological at electric sintering, and thermophysical, related to the materials, necessitates our research in this area.

3. The aim and objectives of the study

The aim of this study is to mathematically describe the heat transfer in the model holder-matrix-upper electrode-punch-sintered sample-bottom electrode-punch-stand.

To accomplish the aim, the following tasks have been set:

– to solve the problem of heating the tooling elements by a control volume method;

– to analyze the calculation results represented by graphic curves.

4. Materials and methods to study thermal effects arising in the tooling elements activated with electric current

4. 1. The studied materials and the equipment used in the experiment

The estimation study in the model holder-dielectric matrix-electrode-punch- sintered ring-shaped product-electrode-punch-stand involved the application of a control volume method. It is one of the most effective among the difference methods to solve the problems of non-stationary thermal conductivity. The problem was solved in the cylindrical coordinate system.

The materials of the mold were made from:

– holder – steel 45;

– dielectric insert – asbestos-cement pipe VT-9;

– needle (hollow inside) – steel KhVG;

– top and bottom electrodes-punches – steel KhVG;

– stand – steel 3.

For experimental measurements:

– temperature – we used contact thermocouples TKhA (chromel-alumel), as well as the loop oscilloscope H 117;

– the pressure of additional pressing and final pressing-the strain amplifier Topaz-3-01 and strain gauges;

– the raw material for the product – chopped BrAZh-9-4 alloy shavings.

5. Results of examining the proposed mathematical model

5. 1. Analysis of thermal flux passage through a control volume

The problem of heat transfer in the model holder-dielectric matrix-electrode-punch-stand was solved by a control volume method. The problem of heating the tooling elements

is solved by a control volume method [16]. A form whose sides are arranged such that the nodal points are in the middle of a square or rectangle is termed the control volume. When splitting an estimated region into a grid, three options for the location of the control volumes are possible [17]: control volume with a reference point is located in the middle, at the border, and in the corner of the estimated zone.

In the calculations, we accept that the thermophysical characteristics, body λ (coefficient of thermal conductivity), γ (density), and C (heat capacity) are constant.

The body temperature at the initial time (τ=0, s) is evenly distributed: $t(r, z, \varphi)$=20 °C. We consider the axisymmetric problem; the coordinate origin is at the point of intersection of the axis and the plane of contact between a water-cooled plate and the upper electrode-punch. The dependence on the temperature in the contact area between the edge of the upper electrode-punch and a stand with water-cooled plates is represented analytically in the following form:

$$t(r, \tau)=t_c=(1-e^{-\alpha\tau}), \quad (1)$$

where t_c and α are the constants (t_c=200 °C, α=0.055 s).

The problem is solved in the cylindrical coordinate system; for the three-dimensional nonstationary thermal conductivity of solids, a general differential equation takes the following form:

$$\gamma c\frac{\partial t(r,\varphi,z)}{\partial\tau}=\lambda\left[\begin{array}{l}\frac{1}{r}\frac{\partial}{\partial r}\left(r\frac{\partial t(r,\varphi,z)}{\partial r}\right)+\\ +\frac{1}{r^2}\frac{\partial^2 t(r,\varphi,z)}{\partial\varphi^2}+\\ +\frac{\partial^2 t}{\partial z^2}(r,\varphi,z)\end{array}\right]+Q_v, \quad (2)$$

where r is the radial coordinate, ϕ is the angular coordinate, z is the axial coordinate, Q_v is the specific heat output of the internal sources of heat at the expense of joule heating.

The distribution of the heat flow has an axial symmetry, so equation (2) will take the following form:

$$\gamma_{i,j}c_{i,j}\left(N-\frac{1}{2}\right)\Delta R^2\Delta z\Delta\varphi\frac{t_N^{n+1}-t_N^n}{\Delta\tau}. \quad (3)$$

In this case, the process of thermal conductivity can be considered two-dimensional, that is, $t=t(r, z, \tau)$. Select a part of the hollow cylinder ABCDEFKL (Fig. 1) with a small enough angle Δφ in the plane of the sector OCD of height Δz.

The speed of changing the heat capacity of the control volume ABCDEFK (in Fig. 2: numbers i=1, j=3) over time Δτ is determined from the ratio

$$\gamma_{i,j}c_{i,j}\left(N-\frac{1}{2}\right)\Delta R^2\Delta z\Delta\varphi\frac{t_N^{n+1}-t_N^n}{\Delta\tau}, \quad (4)$$

where $c_{i,j}$ is the heat capacity of the material of control volume; $\gamma_{i,j}$ is the density of the control volume's material; ΔR is the step along the radial coordinate; Δz is the step along the axial coordinate; Δz is the step in time; n is the sequential number of a time step; t_N^{n+1} is the unknown control volume's temperature over time $\tau=(n+1)\,\Delta\tau$; t_N^n is the known control volume's temperature over the preceding period (Fig. 4).

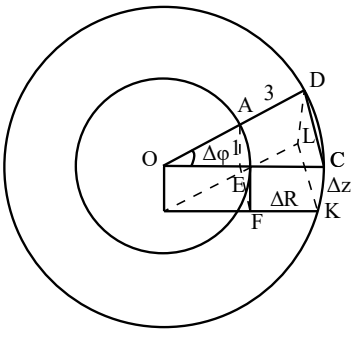

Fig. 1. Overall view of the tooling elements' control volume

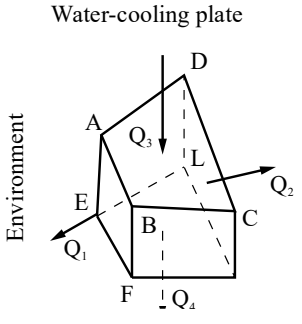

Fig. 2. Schematic passage of heat flows through a control volume

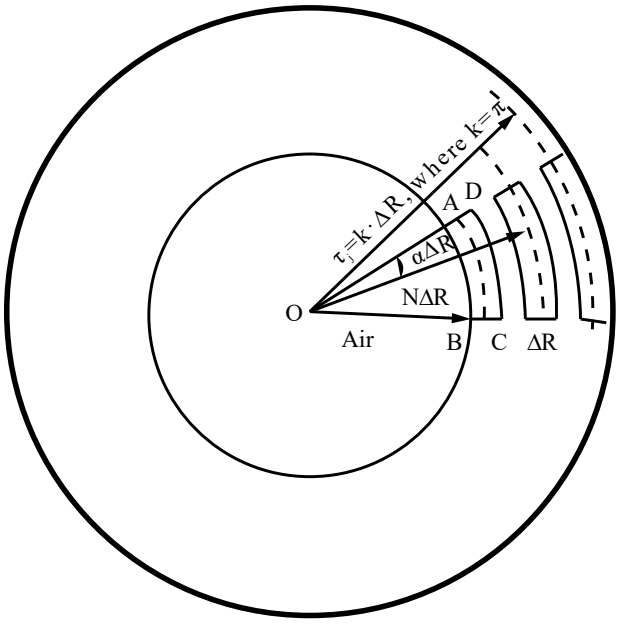

Fig. 3. Schematic passage of heat flows in a radial direction

The heat balance in closed spaces in the tooling's elements is described by the following equation:

$$c_a\gamma_a V_a\frac{\partial t_a}{\partial\tau}=\alpha\left[\begin{array}{l}F_1(t_1-t_{cp})+F_2(t_2-t_{cp})+\\ +F_3(t_3-t_{cp})\end{array}\right], \quad (5)$$

where c_a, γ_a, V_a is the heat capacity, density, volume of air; F_1–F_3 is the area of contact of the tangent layers of air with the inter-

nal walls of the tooling elements, forming the enclosed spaces 1, 2, and 3, respectively; α is the heat transfer coefficient; t_1–t_3 is the temperature of the internal walls of closed volumes.

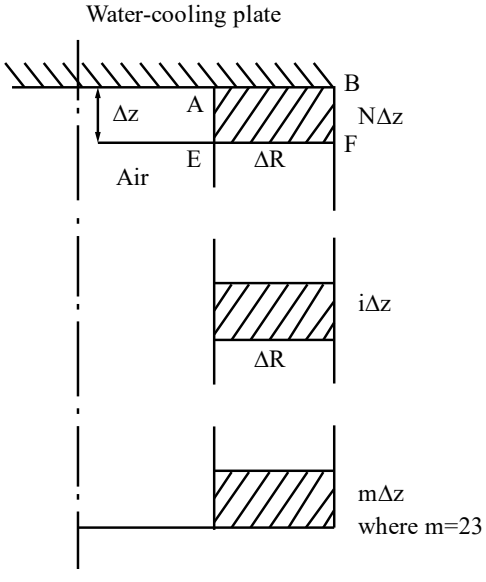

Fig. 4. Schematic passage of heat flows in a vertical direction

The amount of heat Q_1 (Fig. 2, 3), which entered a given volume through the left edge AEFB of area $S_1=N\Delta R\Delta z\Delta\varphi$ in the radial direction, equals:

$$Q_1 = N\Delta R\Delta z\Delta\varphi\alpha_c\left(t_a - t^n_{i,j}\right), \tag{6}$$

where

$$t_A = t_{A_o} + \frac{\Delta\tau\alpha F}{V_A c_A \gamma_A}\left(t_{air} - t_{cp}\right) \tag{7}$$

– the difference expression, where t_A is the air temperature during the sintering process. The amount of heat Q_2, released from a given volume through the right edge LKCД (Fig. 2) of area $S_2=(N+1)\ \Delta R\Delta z\Delta\varphi$ due to thermal conductivity, equals

$$Q_2 = (N+1)\Delta R\Delta z\Delta\varphi\frac{\left(t^n_{i,j} - t^n_{i,j+1}\right)}{\frac{\Delta R}{2\lambda_{i,j}} + \frac{\Delta R}{2\lambda_{i,j+1}}}, \tag{8}$$

where the following expression

$$\left(\frac{\Delta R}{2\lambda_{i,j}} + \frac{\Delta R}{2\lambda_{i,j+1}}\right) \tag{9}$$

is derived based on the following considerations (Fig. 3).

The heat flows per unit area of two control volumes (1 and 2) will take the form of the following equation:

$$Q_{un.} = \lambda_{i.j} + \frac{t^n_{i,j+\frac{1}{2}} - t^n_{i,j}}{\frac{\Delta R}{2}} = \lambda_{i,j+1}\frac{t^n_{i,j+1} - t^n_{i,j+\frac{1}{2}}}{\frac{\Delta R}{2}}, \tag{10}$$

subject to the condition of the heat flow discontinuity at the interface of the distribution of the heated (1) and unheated (2) zones of the body intersection.

Transform equation (10)

$$\lambda_{i,j}t^n_{i,j+\frac{1}{2}} - \lambda_{i,j}t^n_{i,j} = \lambda_{i,j+1}t^n_{i,j+\frac{1}{2}} \tag{11}$$

or

$$\left(\lambda_{i.j} + \lambda_{i,j+1}\right)t^n_{i,j+\frac{1}{2}} = \lambda_{i,j+1}t^n_{i,j} + \lambda_{i,j}t^n_{i,j}. \tag{12}$$

From (12), we find the desired value

$$t^n_{i,j+\frac{1}{2}} = \frac{\lambda_{i,j+1}t^n_{i,j} + \lambda_{i,j}t^n_{i,j}}{\lambda_{i,j} + \lambda_{i,j+1}}. \tag{13}$$

Substitute the value

$$t^n_{i,j+\frac{1}{2}},$$

using (6), into the expression for the summary flow $Q_{un.}$ of two control volumes:

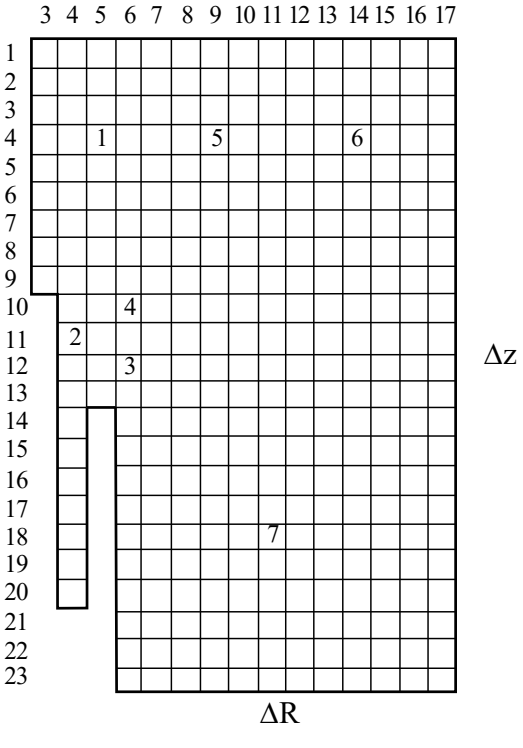

Fig. 5. The intersection of the tooling elements divided into 318 control volumes: 1 – upper electrode-punch, 2 – needle, 3 – bottom electrode-punch, 4 – sintered product, 5 – asbestos-cement matrix-insert, 6 – holder, 7 – stand

$$\begin{aligned}
Q_{un.} &= 2\lambda_{i,j}\frac{1}{\Delta R}\left(\frac{\lambda_{i,j+1}t^n_{i,j+1} + \lambda_{i,j}t_{i,j}}{\lambda_{i,j} + \lambda_{i,j+1}} - t^n_{i.j}\right) = \\
&= \frac{2\lambda_{i,j}}{\Delta R}\left(\frac{\lambda_{i,j+1}t^n_{i,j+1} + \lambda_{i,j}t_{i,j} - t^n_{i,j}\lambda_{i,j}}{\lambda_{i,j} + \lambda_{i,j+1}} - \frac{\lambda_{i,j+1}t^n_{i,j}}{\lambda_{i,j} + \lambda_{i,j+1}}\right) = \\
&= \frac{2\lambda_{i,j}\lambda_{i,j+1}}{\Delta R}\frac{t^n_{i,j+1} - t^n_{i,j}}{\lambda_{i,j} + \lambda_{i,j+1}} = \\
&= \frac{2}{\Delta R}\frac{t^n_{i,j+1} - t^n_{i,j}}{\frac{2\lambda_{i,j}}{\lambda_{i,j} + \lambda_{i,j+1}} + \frac{\lambda_{i,j+1}}{\lambda_{i,j} + \lambda_{i,j+1}}} = \frac{t^n_{i,j+1} - t^n_{i,j}}{\frac{\Delta R}{2\lambda_{i,j}} + \frac{\Delta R}{2\lambda_{i,j+1}}},
\end{aligned} \tag{14}$$

where $\lambda_{i,j}$ and $\lambda_{i,j+1}$ are the thermal conductivity of two control volumes (Fig. 6).

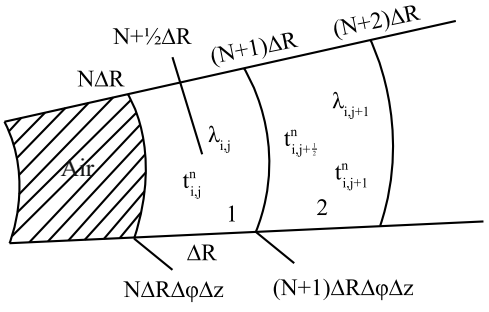

Fig. 6. Determining the coefficient of thermal conductivity of two control volumes

The amount of heat Q_3, which arrives due to the thermal conductivity in a vertical direction through the upper edge ABCD (Fig. 2, 3) of area

$$S_3 = \left(N + \frac{1}{2}\right)(\Delta R)^2 \Delta\varphi \tag{15}$$

equals

$$Q_3 = \left(N + \frac{1}{2}\right)(\Delta R)^2 \Delta\varphi \frac{t^n_{i,j} - t_{i+1,j}}{\frac{\Delta z}{2\lambda_{i,j}} + \frac{\Delta z}{2\lambda_{i+1,j}}}. \tag{16}$$

5. 2. Analysis of the internal sources of heat by joule heating

The amount of heat that is released inside the control volumes by Joule heating Q can be represented as follows:

$$Q = k'lU\tau, \tag{17}$$

where U is the voltage applied to other elements of the tooling (the upper and bottom electrode-punch, needle, and stand), I is the amperage, τ is the time of the progress of electric current, k' is the parameter that takes into consideration the level of usable heating (we accept it equal to 0.6).

On the other side

$$Q = Q_x + Q_y, \tag{18}$$

where Q_x is the amount of heat released in the elements of the metal tooling, Q_y is the amount of heat released in the sintered products.

Proceeding from the equivalent replacement scheme of the metal tooling unit (electrodes-punches and needle) and the sintered product shown in Fig. 7, we derive the following formula:

$$Q_x + Q_y = q_1 + q_2 + q_3 + q_4, \tag{19}$$

where q_1–q_4 is the amount of heat that is released on each electrical resistance R_1–R_4 by joule heating (here, R_1 is the resistance of the upper electrode-punch, R_2 is the electrical resistance of the sintered product, R_3 is the electrical resistance of the needle's area, tangent to the sintered product, R_4 is the electrical resistance of the bottom electrode-punch and the needle's area in contact with it).

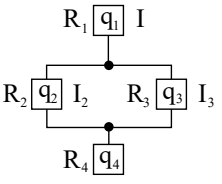

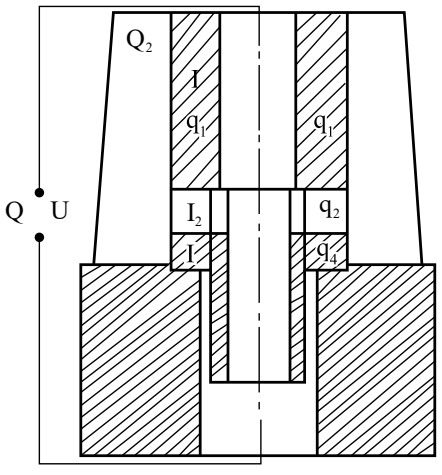

Fig. 7. The equivalent scheme of substituting a unit of elements of the metal tooling (electrodes-punches and needle) and the sintered product

Find q_1–q_4:

$$q_1 = I_1^2 R_1 \tau,$$

$$q_3 = I_3^2 R_3 \tau, \tag{20}$$

$$q_2 = I_2^2 R_2 \tau,$$

$$q_4 = I_4^2 R_4 \tau,$$

where, according to the Kirchhoff law

$$I_2 = \frac{IR_3}{R_2 + R_3},$$

$$I_3 = \frac{IR_2}{R_2 + R_3}. \tag{21}$$

Define Q_x and Q_y from the values of q_1–q_4:

$$Q_x = q_1 + q_3 + q_4;$$

$$Q_y = q_2. \tag{22}$$

The specific heat output of internal heat sources in the elements of metal tooling Q_{V1} and the sintered product Q_{V2} is equal to:

$$Q_{V1} = \frac{Q_x}{V_x}, \tag{23}$$

where V_x is the total volume of the electrodes-punches and needle;

$$Q_{V2} = \frac{Q_y}{V_y}, \tag{24}$$

where V_y is the volume of the sintered product.

5. 3. Deriving a general heat balance equation

Thus, we obtain the equation of heat balance of the control volumes in a general form:

$$c_{i,j}\gamma_{i,j}\left(N-\frac{1}{2}\right)(\Delta R)^2\Delta z\Delta\varphi\left(t_N^{n+1}-t_N^n\right)=$$
$$=N\Delta R\Delta z\Delta\varphi\left(t_c-t_{i,j}\right)-(N+1)\Delta R\Delta z\Delta\varphi\times$$
$$\times\frac{\left(t_{i,j}^n-t_{i,j+1}^n\right)}{\frac{\Delta R}{2\lambda_{i,j}}+\frac{\Delta R}{2\lambda_{i,j+1}}}+\left(N+\frac{1}{2}\right)(\Delta R)^2\Delta\varphi\times$$
$$\times\frac{\left(t_n-t_{i,j}\right)}{\frac{\Delta z}{2\lambda_n}+\frac{\Delta z}{2\lambda_{i,j}}}-\left(N+\frac{1}{2}\right)(\Delta R)^2\Delta\varphi\times$$
$$\times\frac{\left(t_{i,j}^n-t_{i+1,j}^n\right)}{\frac{\Delta z}{2\lambda_{i,j}}+\frac{\Delta z}{2\lambda_{i+1,j}}}+\left(N+\frac{1}{2}\right)(\Delta R)^2\Delta z\Delta\varphi Q_V. \quad (25)$$

The i, j indices for different areas (press-tool components and a sintered product) change in the following limits:

– upper electrode-punch ($3\equiv j\equiv 6;1\equiv i\equiv 9$);
– bottom electrode-punch ($5\equiv j\equiv 6$; $i\equiv 13$);
– needle ($j\equiv 4;10\equiv i\equiv 20$);
– the sintered product ($5\equiv j\equiv 6;10\equiv i\equiv 12$);
– asbestos-cement matrix-insert ($7\equiv j\equiv 11;1\equiv i\equiv 9$);
– holder ($12\equiv j\equiv 17;1\equiv i\equiv 13$);
– stand ($6\equiv j\equiv 17;14\equiv i\equiv 23$).

The intersection of the tooling elements with the sintered product (Fig. 5) is divided into 318 control volumes. For each control volume, it is necessary to build a heat balance equation. However, for many volumes, the equations are identical: ultimately, one can record 19 types of heat balance equations.

Table 1 summarizes the output data for calculation.

The porosity of a multi-component powder ring sample is accounted for by the following ratio [19]:

$$\gamma=\gamma_0(1-\theta);\ \ c=c_0(1-\theta), \quad (26)$$

$$\lambda=\lambda_0\left(1-\frac{3}{2}\theta\right);\ \ \frac{1}{S}=\left(\frac{1-\frac{3}{2}\theta}{S_0}\right), \quad (27)$$

where Θ is the porosity of the sintered sample in the fractions of unity (characters with a zero index indicate characteristics of a nonporous material, without the index – a porous material):

$$\gamma_0=\sum_{i=1}^{n}U_i\gamma_0^{(i)};\ \ \lambda_0^{\frac{1}{3}}=\sum_{i=1}^{n}U_i\lambda_0^{(i)\frac{1}{3}};$$
$$c_0=\sum_{i=1}^{n}U_ic_0^{(i)};\ \ \frac{1}{S_0^{\frac{1}{3}}}=\sum_{i=1}^{n}\frac{U_i}{S_0^{(i)\frac{1}{3}}}, \quad (28)$$

where U is the volumetric fraction (fractions of unity) of the i-th component, c_0, λ_0, γ_0, and s_0 is its density, heat capacity, thermal conductivity, and electrical resistivity, respectively.

The derived expression of heat balance for control volumes in a general form makes it possible to describe the heat distribution in all elements of the tooling, as well as to optimize the selection of materials contributing to the concentration of usable heating in the area of the sintered product.

Table 1

The thermophysical characteristics of the tooling elements and a sintered product

Tooling element	Material	Electro- and thermophysical characteristics			
		Density, kg/m^3	Heat capacity, J/kg, °C	Heat conductance, J/m·s, °C	Specific electrical resistance, Ohm·mm^2/m
Upper electrode-punch	Steel KhVG	7,800	571.2	29.4	0.271
Needle	Steel KhVG	7,800	571.2	29.4	0.271
Bottom electrode-punch	Steel KhVG	7,800	571.2	29.4	0.271
Matrix-insert	Asbestos-cement	2,500	815	0.37	–
Holder	Duralumin	2,700	940	155	–
Stand	Steel 45	7,800	470	48	–
Sintered product (shavings from a cast rod) with alloying powder additives	BrAZh-9-4	7,500	400	88	0.125
	copper	8,900	380	410	0.169
	graphite	2,300	836	0.4	10
Sintered product considering porosity	–«–	6,433	370	68	0.171

We show the numerical calculation for a regime with the sintering time of 90 s, with the amount of heat released due to joule heating per unit volume of the elements of metal tooling Q_{V1}=3,250 J/cm, per unit of product volume Q_{V2}=3,080 J/cm.

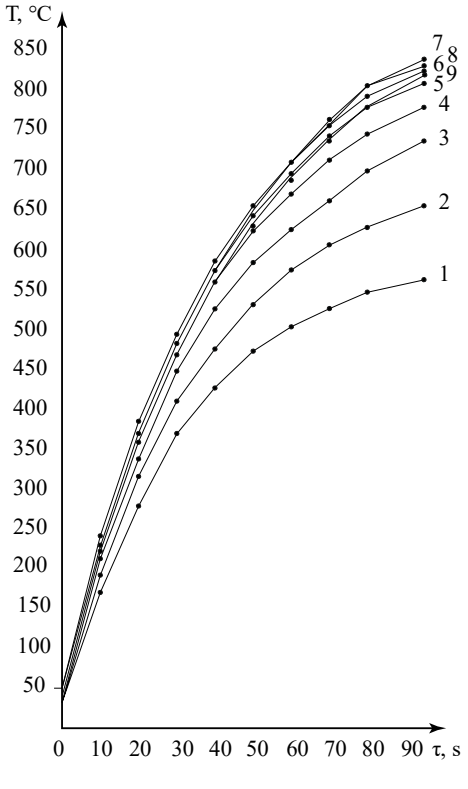

Fig. 8. Time dependence of the temperature of the upper electrode-punch at heating with electric current

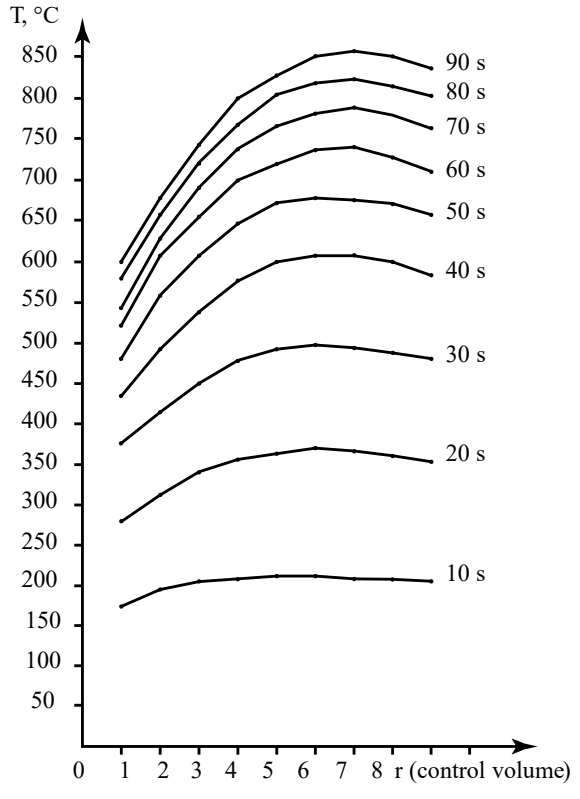

Fig. 9. Spatial dependence of the upper electrode-punch temperature at heating with electric current

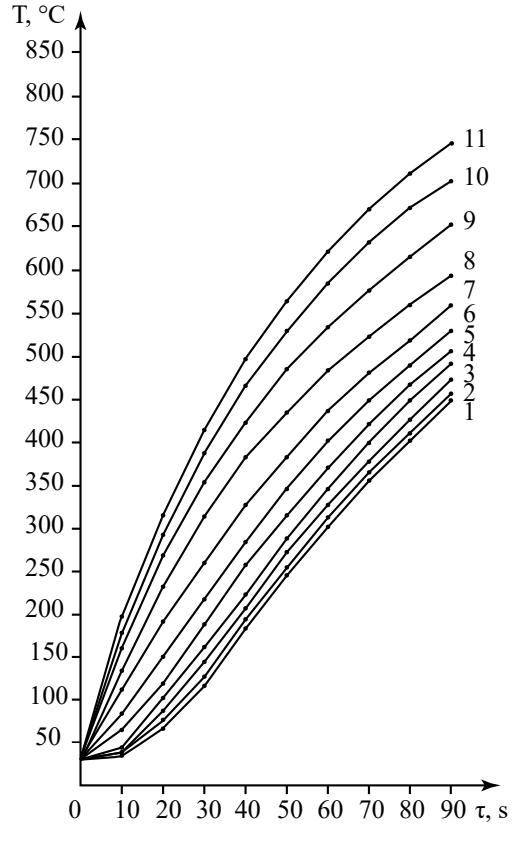

Fig. 10. Time dependence of the needle temperature at heating with electric current

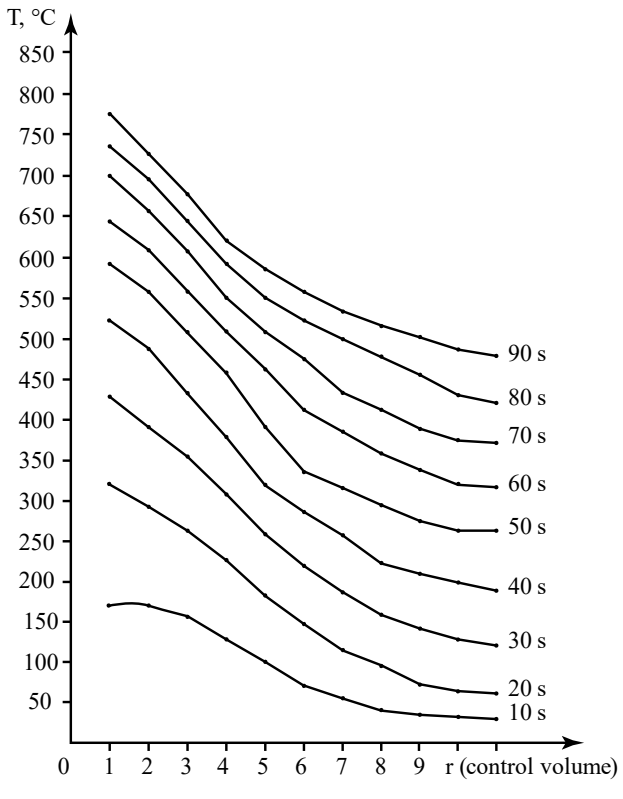

Fig. 11. Spatial dependence of the needle temperature at heating with electric current

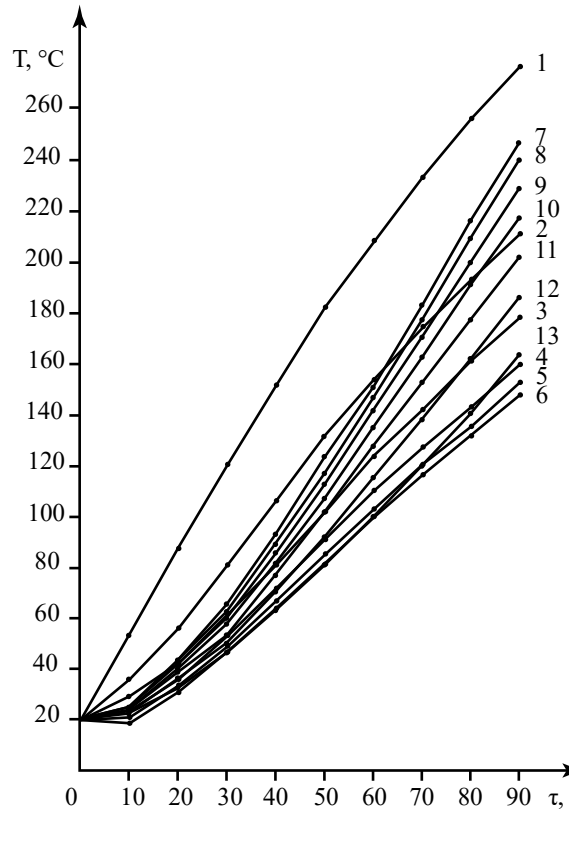

Fig. 12. Time dependence of the temperature of an asbestos-cement matrix-insert when heating with electric current the sintered part and metallic components of the press tool

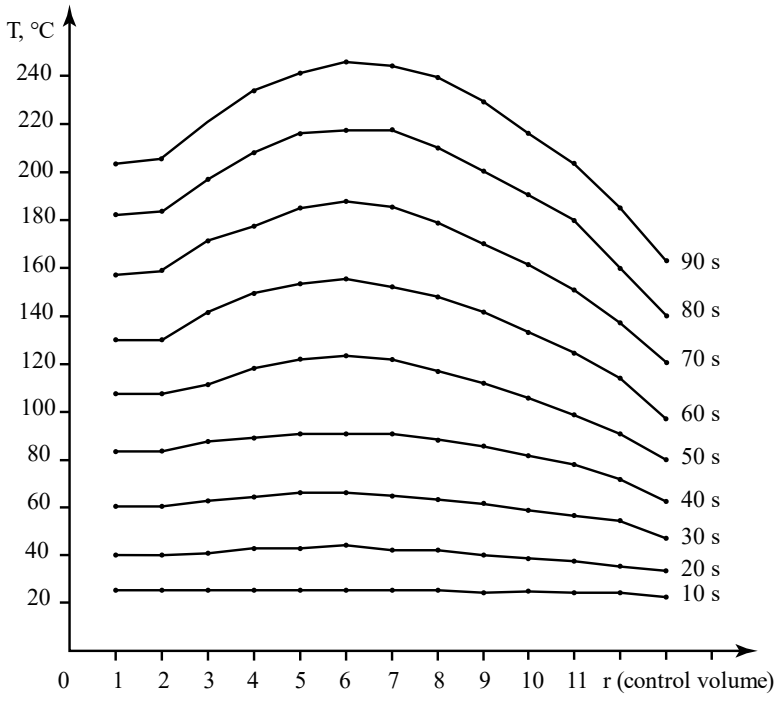

Fig. 13. Spatial dependence of the temperature of an asbestos-cement matrix-insert at heating with electric current

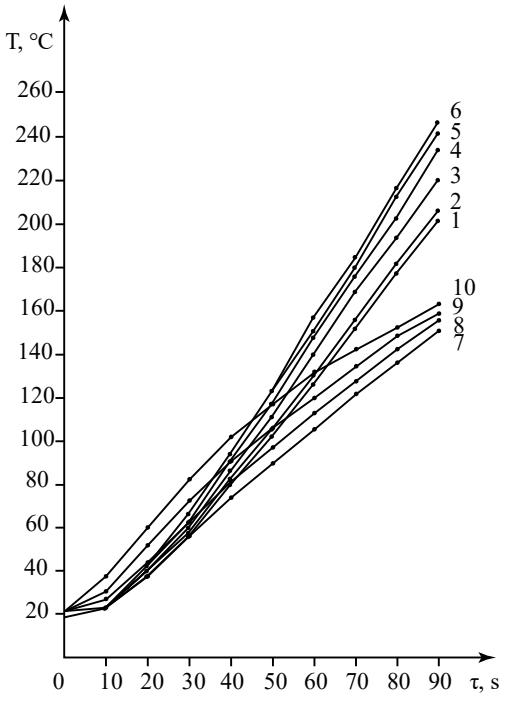

Fig. 15. Time dependence of the steel stand temperature at heating with electric current

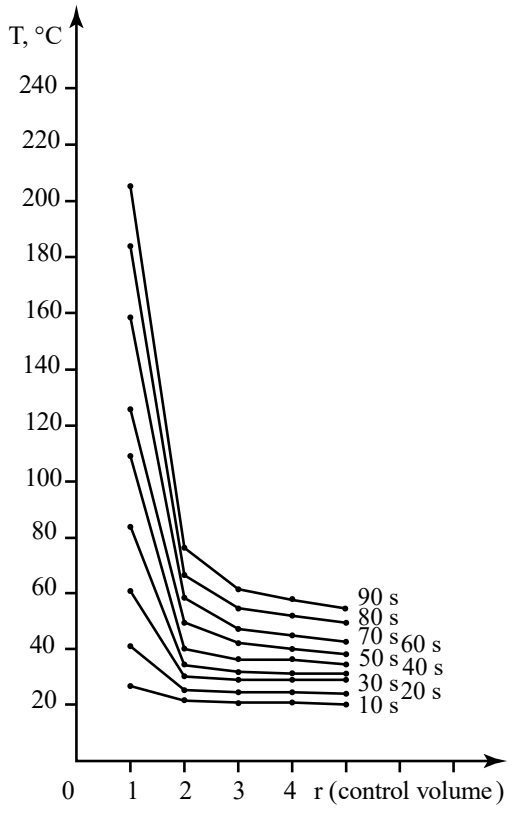

Fig. 14. The radial spatial dependence of the temperature of an asbestos-cement matrix-insert at heating with electric current

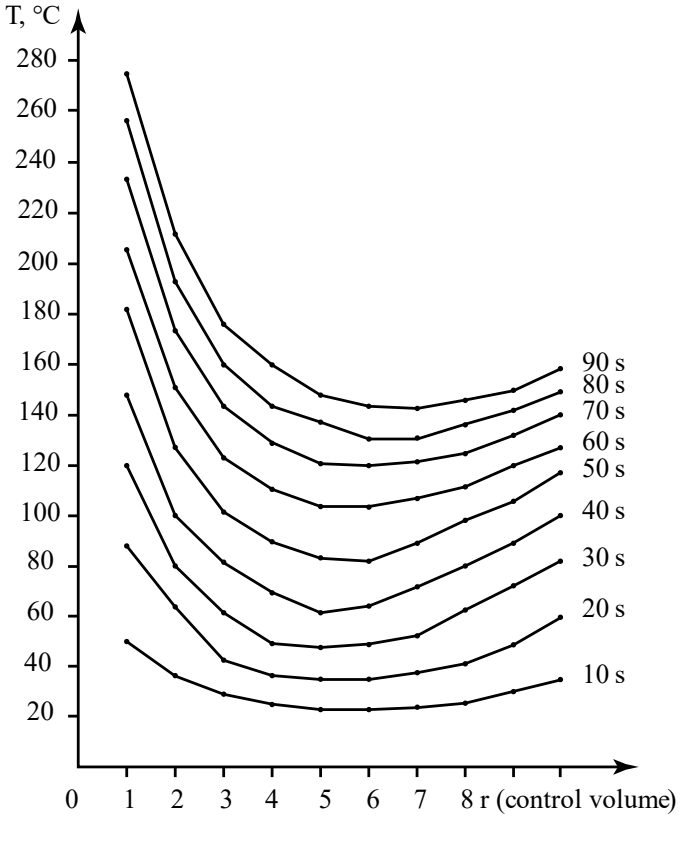

Fig. 16. Spatial dependence of the steel stand temperature at heating with electric current

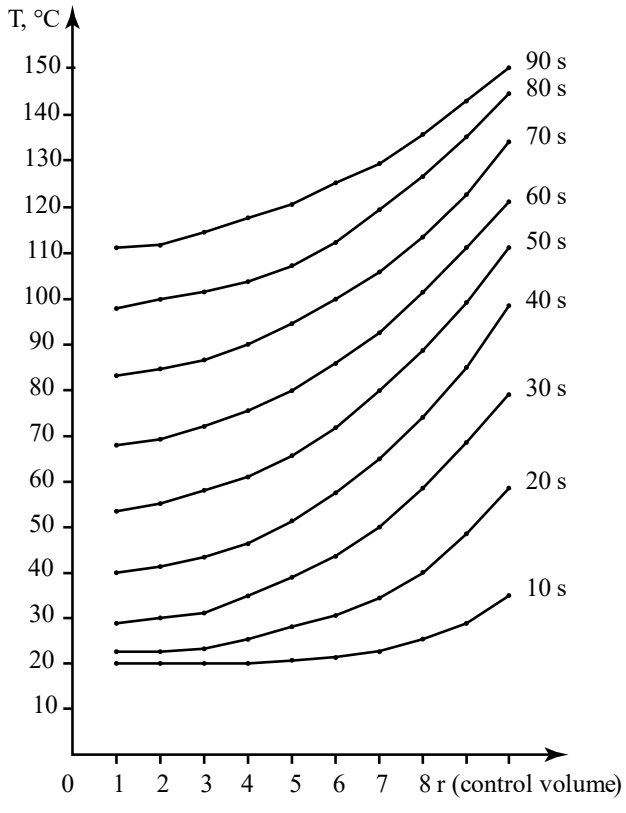

Fig. 17. The axial spatial dependence of the steel stand temperature for the region with coordinates j=17;14≤i≤23

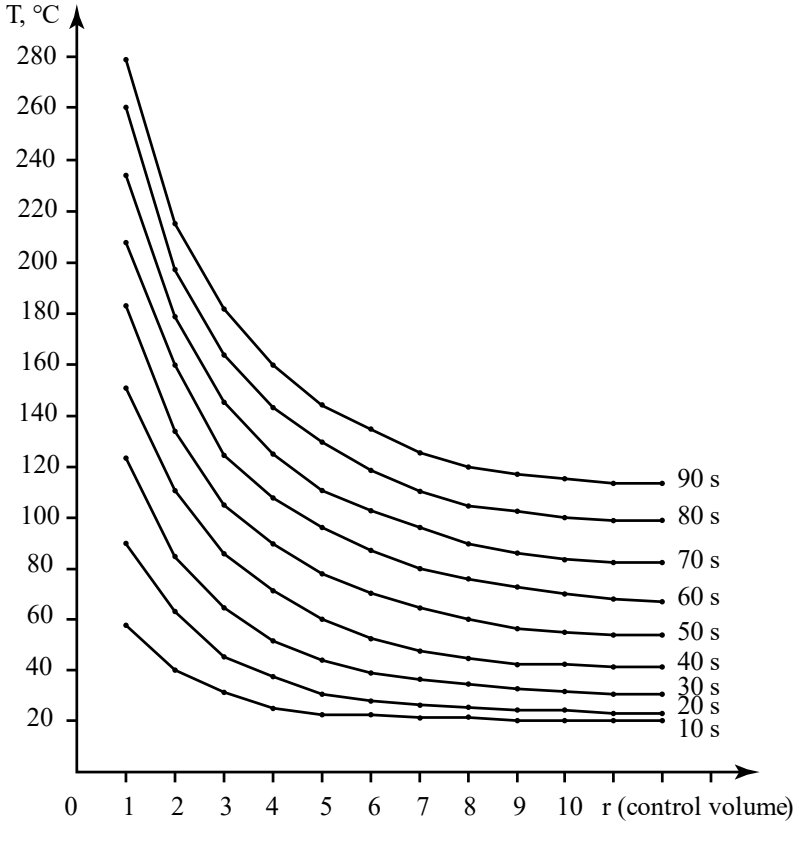

Fig. 18. The radial spatial dependence of the steel stand temperature

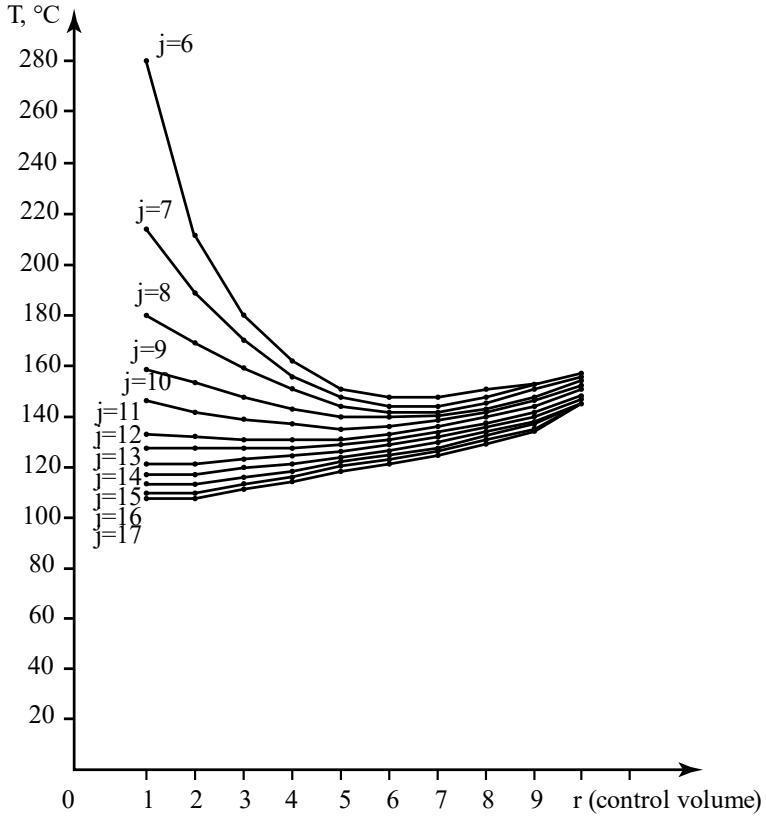

Fig. 19. The spatial dependence of temperature at a fixed time value (t=90 °C) for region 14≡i≡23

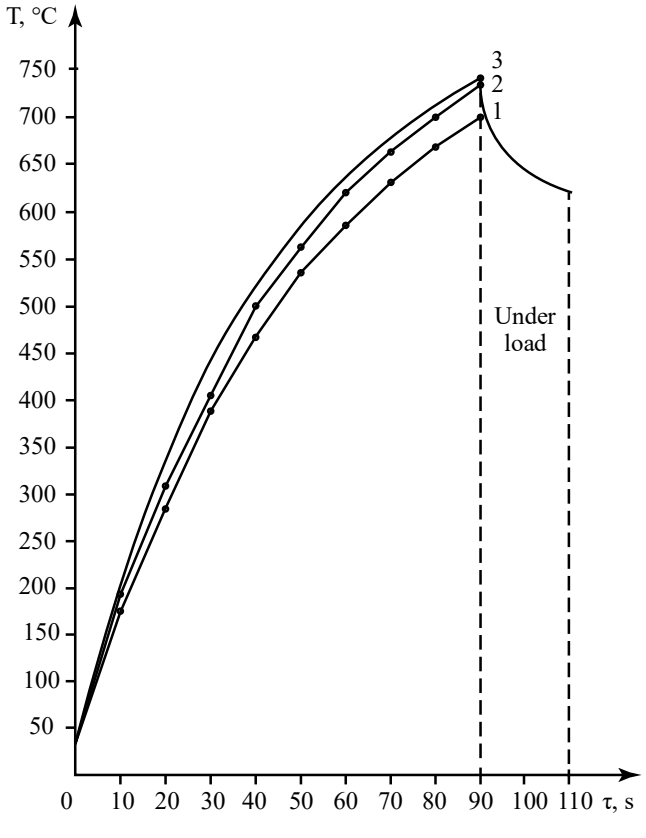

Fig. 20. The time dependence of the sintered product temperature at heating with electric current

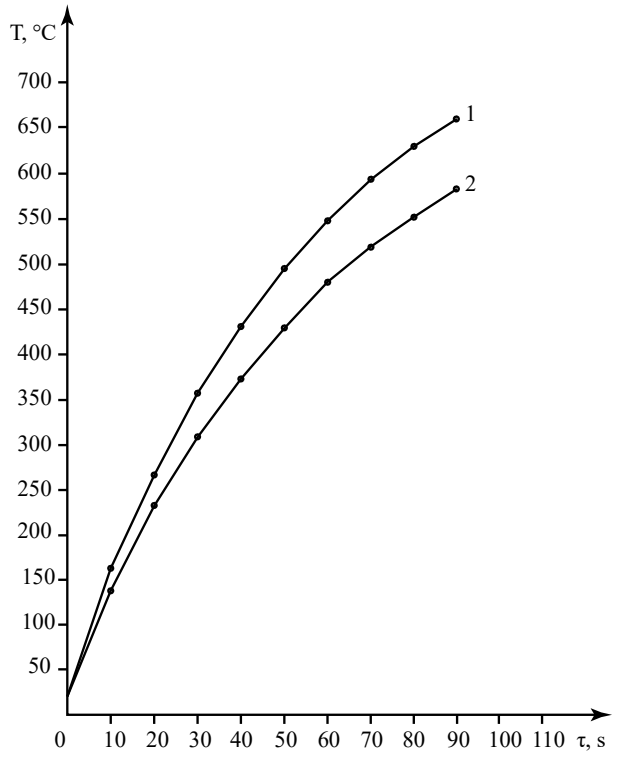

Fig. 21. The time dependence of the bottom electrode-punch temperature at heating with electric current

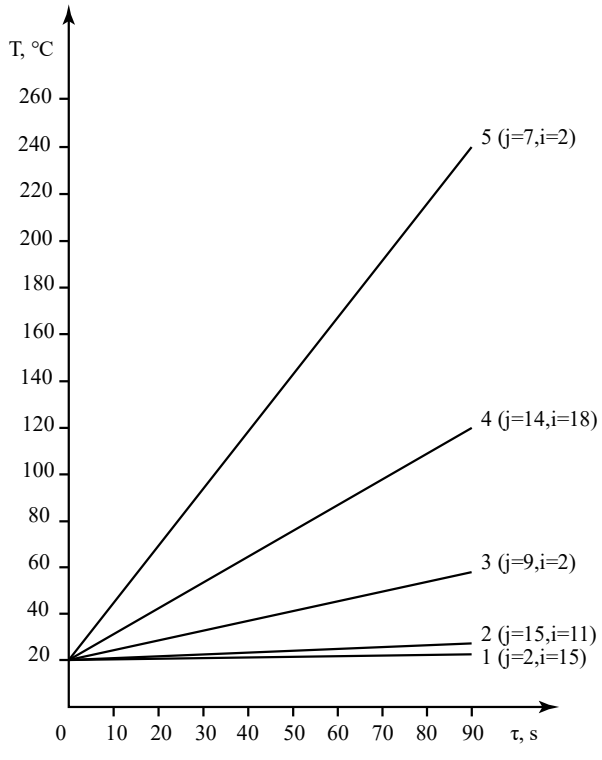

Fig. 23. Experimental time dependence of the tooling elements temperature at heating them with electric current

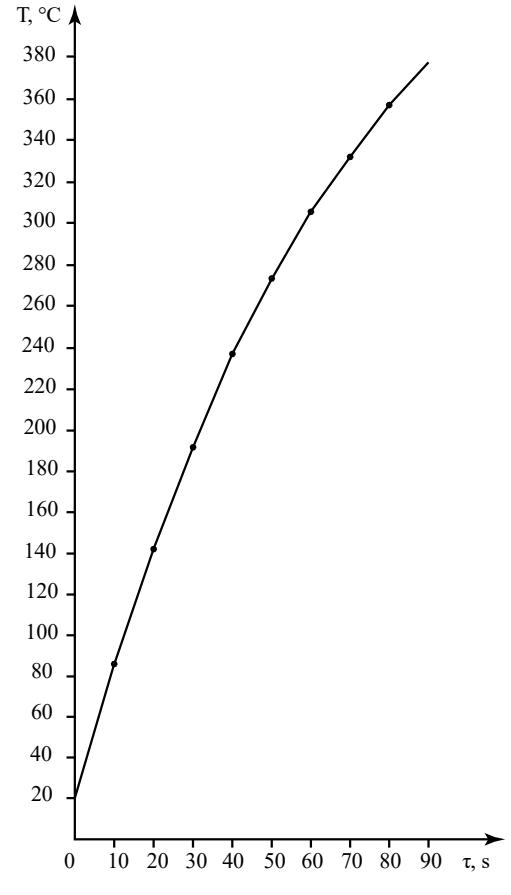

Fig. 22. The time dependence of the temperature of the air, which is in a closed volume of the mold, at heating with electric current

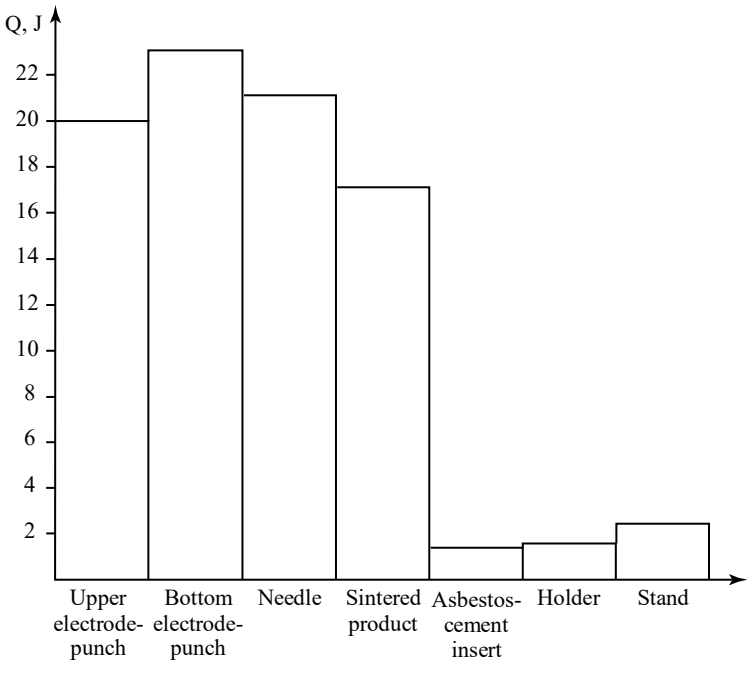

Fig. 24. The balance of heat distribution, which is released per unit volume of the tooling elements and a sintered product, per unit time

6. Discussion of results of studying the modeling of the process of heating the tooling elements

The calculation results are represented in Fig. 8–24. As the heat is spread to the sintered object relative to the height of the upper electrode-punch (Fig. 8) (coordinates j=3,

1≡*i*≡9), the temperature gradually increases in sections 1–7 and reaches its maximum, which is 845 °C. There is a further noticeable tendency towards decreasing in the areas close to the product (curves 8.9), to temperature 823 °C. This might be due to the complex influence between the electric- and thermophysical properties of the electrode-punch material and the sintered powder and the balance of heat-generating processes, its inflow and outflow [20]. Fig. 8 shows the time-based and, in Fig. 6, space-based dependences of the upper electrode-punch temperature.

To reduce the weight of the tooling and to warm faster its components (the upper electrode-punch and needle), the latter are executed hollow. A movable needle forms the inner wall of the sintered bushing and warms up at the end of the process in this area to a mean temperature of 73 °C. Fig. 10 shows the monotonous decrease in temperature along the needle height (*j*=4; 10≡*i*≡20) over time. The temperature of the needle in the area surrounded by air decreases less intensively due to the slight convective heat exchange caused by the hot air within a closed volume (Fig. 11).

In the contact area of the internal walls of an asbestos-cement matrix with the upper electrode-punch (*j*=7; 1≡*i*≡9) for time dependences (Fig. 12) including the control volume with the coordinate *i*=6, the temperature rises; its maximum value reaches 248 °C. When approaching the sintered product, it begins to fall (curves 7–9) and, in the area of the contact between the wall and the bottom electrode-punch, the temperature reaches 166 °C (curve 13).

A high-quality pattern is demonstrated by the axial and radial spatial dependences of the asbestos-cement matrix-insert when heating with electric current (Fig. 13, 14).

It is known that asbestos fibers undergo a series of changes during thermal treatment that affect their physical properties [21]. In the case of prolonged aging at a temperature of 110 °C, a significant part of the adsorptive water is released, thereby decreasing the mechanical strength of asbestos fibers, thus predetermining the wear of the matrix. When moving in the radial direction from the object of sintering, the heating of an asbestos-cement insert becomes less intense; the temperature of its internal layers reaches 20–35 °C (Fig. 14).

The temperature of the steel stand (*j*=6;14≡*i*≡23) at the end of the process, when moving away from the lower electrode-punch (Fig. 15), varies in the range of 279 °C to 147 °C (curves 1–6). Then there is a gradual increase in it when approaching the lower water-cooling plate (curves 7–10). A very pronounced indication of the change in the temperature of the stand is provided by its spatial dependence (Fig. 16) for each time interval. Fig. 17 shows a temperature change for a series of control volumes (*j*=17; 14≡*i*≡23) of the stand. In this case, the temperature of the control volume (*j*=17; *i*=14) in the area of contact with a duralumin holder (between them is an air gap of thickness 2...3 mm), due to the lack of joule heating, is slightly less and, over time, changes from 150 to 35 °C. Th stand contacts the bottom electrode-punch, asbestos-cement matrix-insert, and holder; the distribution of temperature in the radial direction in these areas is characterized by the curves that monotonously descend (Fig. 18).

The dependences of temperature on the axial coordinate in a steel stand near the inner air cavity demonstrate maxima; as the distance grows, towards the periphery, the curves acquire a monotonous ascending character (Fig. 19).

For the vertical zone *j*=6, in the contact area with the lower electrode-punch, the maximum temperature is observed, 278 °C. As the distance from the source of joule heating grows, the temperature monotonously decreases in the area 14≡*i*≡21 to 146 °C, and, in the zone in contact with the bottom water-cooled plate (21≡*i*≡23), there is a tendency to increase to 158 °C. It seems this is due to the mass of the stand and scattering of the heat flow [22, 23].

The estimated value of temperature in the upper and lower layers of the sintered product (chip powder BrAZh-9-4) (Fig. 20, curves 1.2) with coordinates *j*=5; 10≡*i*≡11 changes at the end of the process from 747 °C to 714 °C [24]. Curve 3 illustrates the experimental dependence of temperature on time, the value of which reaches 750 °C. The character of the curve is the same as that in the estimated dependences. After 90 s, the final pressure was applied over 20 s and the temperature fell to 635 °C [25].

The time dependence of the lower electrode temperature is similar to the above dependence (Fig. 21; *j*=5; 12≡*i*≡13), however, at the end of the process, it is heated to a slightly lower temperature: for *i*=12, to 650 °C; for *i*=13, to 575 °C. The mold has a closed inner space, inside which there is a certain amount of air. The exchange of air with the environment is almost absent. Because of the very weak convective heat exchange, the mass of air heats up quickly (Fig. 22), which plays its role in the heating of the tangent parts of the metal tooling. Thus, at the end of the process, the air is heated to a temperature of 378 °C.

A change in the temperature of the holder is insignificant and the estimated value reaches 22–23 °C; in the zone in contact with a steel stand, 32 °C. Experimental measurements showed that in the upper half of the holder the temperature increases from 25 to 26 °C (Fig. 23, curve 1); at the bottom – from 27 to 29 °C (curve 2).

The thermocouples helped register the temperature of the asbestos-cement matrix at points with coordinates *j*=8; *i*=2 and *j*=9; *i*=2 240 and 60 °C (Fig. 23, curves 3 and 5). For example, the estimated value of the temperature at point (*j*=8; *i*=2) is 240 °C; at the same time, experimental – 223 °C.

For the steel stand at a point with coordinates *j*=14; *i*=18, the estimated temperature was 123 °C, experimental – 120 °C (Fig. 23, curve 4).

Based on the derived heat balance for the control volumes in a general form, we have the distribution of the latter in the tooling elements (Fig. 24).

The advantage of a control volume method (CVM) is that it is based on the macroscopic physical laws, it includes the exactly integrated preservation of values such as mass, pulse, and energy, in any group of control volumes. A solution that is obtained using a CVM will always keep the energy balance over the entire estimated area, which cannot be said about the solutions derived by using other methods. The absolute advantages of a given method are the high efficiency and simplicity of implementation, as well as the visibility of the sampling rate procedure, which makes it possible to construct the high-order precision schemes. However, these benefits are realized only when applying a regular enough (structured) grid – almost orthogonal and with smoothly changing cell sizes. Consequently, most CVM applications are limited to the cases of estimated areas that are quite simple in terms of geometry.

The current study is to be advanced by using more wear-resistant materials, specifically the replacement, in

the future, of an asbestos-cement insert with materials with dielectric coatings. Constraints in obtaining future experimental results may await researchers at the stage of registering control parameters at electric sintering because of the possibility of the occurrence of undesirable electro-physical effects.

Preliminary modeling of the process of the activated treatment with an electric current of powder products would allow a more expedient choice of tooling materials and the optimization of a future technological cycle.

This research is not a continuation of an earlier one; however, we are going to improve it in the future.

7. Conclusions

1. Our analytical research has solved the problem of heating in the elements of the mold: holder-asbestos-cement insert-upper electrode-punch-sintered sample-lower electrode-punch-stand, by deriving a heat balance equation for the latter in a general form. The resulting expression for the tooling control volumes makes it possible to describe the heat distribution in all elements of the tooling, as well as to optimize the choice of materials that could promote the concentration of usable heating in the zone of a sintered product.

2. Our mathematical description of heat distribution in the considered model has made it possible to establish the overall pattern of changes in temperature fields according to the graphic curves shown in Fig. 8–24. Special features of their formation are as follows:

– the spatial and time dependences of the upper electrode-punch temperature are nonlinear in character, it mostly increases; there is probably an intensive heat outflow in areas close to the product;

– a decrease in the temperature of the movable needle occurs throughout the entire process of sintering; in the part surrounded by air, it is less intense;

– for the case of prolonged aging in the matrix at a temperature of 110 °C, a significant portion of the adsorptive water is released, the mechanical strength of asbestos fibers decreases, thus causing the wear of the matrix;

– the estimated values of temperature in the upper and lower layers of the sintered product are quite close and differ little from experimental; they change at the end of the process from 747 °C to 714 °C;

– the sintered product concentrates 24 % of the thermal energy released from the entire "node" (press-tool-product).

The considered mathematical model enables the targeted adjustment of temperature fields by preliminary calculation and choosing the tooling materials based on the thermal-physical characteristics.

References

1. Morozov, A. S., Raychenko, A. I. (1988). Nekotorye strukturnye osobennosti materialov, poluchennyh elektrospekaniem droblennoy struzhki alyuminievoy bronzy. Elektronnaya obrabotka materialov, 5, 38–41.
2. Morozov, A. S., Burenkov, G. L., Raychenko, A. I., Tomchak, N. N., Lysakovskiy, N. I. (1987). Vliyanie stepeni okislennosti na strukturu i svoystva materiala poluchennogo elektricheskim spekaniem struzhkovogo poroshka alyuminievoy bronzy. Poroshkovaya metallurgiya, 10, 44–48.
3. Raychenko, A. I., Chernikova, E. S. (1989). Matematicheskaya model' elektricheskogo nagreva poristoy sredy sovmestno s podvodyashchimi elektrodami-punsonami. Poroshkovaya metallurgiya, 5, 34–41.
4. Pilipchenko, A. V., Tsitrin, A. I., Homenko, A. N. (1987). Modelirovanie temperaturnogo polya pri pryamom elektricheskom nagreve poroshkovyh materialov. Poroshkovaya metallurgiya, 3, 26–29.
5. Kreyt, F., Bllek, U. (1983). Osnovy teploperedachi. Moscow: Mir, 512.
6. Samarskiy, A. A. (1971). Vvedenie v teoriyu raznostnyh shem. Moscow: Nauka, 552.
7. Zhang, Z.-H., Liu, Z.-F., Lu, J.-F., Shen, X.-B., Wang, F.-C., Wang, Y.-D. (2014). The sintering mechanism in spark plasma sintering – Proof of the occurrence of spark discharge. Scripta Materialia, 81, 56–59. doi: https://doi.org/10.1016/j.scriptamat.2014.03.011
8. Milligan, J., Shockley, J. M., Chromik, R. R., Brochu, M. (2013). Tribological performance of Al–12Si coatings created via Electrospark Deposition and Spark Plasma Sintering. Tribology International, 66, 1–11. doi: https://doi.org/10.1016/j.triboint.2013.04.006
9. Jin, X., Gao, L., Sun, J. (2010). Highly Transparent Alumina Spark Plasma Sintered from Common-Grade Commercial Powder: The Effect of Powder Treatment. Journal of the American Ceramic Society, 93 (5), 1232–1236. doi: https://doi.org/10.1111/j.1551-2916.2009.03544.x
10. Kolomeichenko, A. V., Kuznetsov, I. S., Kravchenko, I. N. (2015). Investigation of the thickness and microhardness of electrospark coatings of amorphous and nanocrystalline alloys. Welding International, 29 (10), 823–825. doi: https://doi.org/10.1080/09507116.2014.986892
11. Kumar, P., Parkash, R. (2016). Experimental investigation and optimization of EDM process parameters for machining of aluminum boron carbide (Al–B4C) composite. Machining Science and Technology, 20 (2), 330–348. doi: https://doi.org/10.1080/10910344.2016.1168931
12. Rafi, H. K., Starr, T. L., Stucker, B. E. (2013). A comparison of the tensile, fatigue, and fracture behavior of Ti–6Al–4V and 15-5 PH stainless steel parts made by selective laser melting. The International Journal of Advanced Manufacturing Technology, 69 (5-8), 1299–1309. doi: https://doi.org/10.1007/s00170-013-5106-7
13. Zuo, F., Saunier, S., Marinel, S., Chanin-Lambert, P., Peillon, N., Goeuriot, D. (2015). Investigation of the mechanism(s) controlling microwave sintering of α-alumina: Influence of the powder parameters on the grain growth, thermodynamics and densification kinetics. Journal of the European Ceramic Society, 35 (3), 959–970. doi: https://doi.org/10.1016/j.jeurceramsoc.2014.10.025
14. Raychenko, A. I., Chernikova, E. S. (1989). Teoreticheskiy analiz nagreva psevdosplavov putem propuskaniya elektricheskogo toka. Poroshkovaya metallurgiya, 7, 15–17.

15. Grigoriev, E., Rosliakov, A. (2007). Electro Discharge Compaction of WC-Co Composite Material Containing Particles of Diamond. Materials Science Forum, 534-536, 1181–1184. doi: https://doi.org/10.4028/www.scientific.net/msf.534-536.1181
16. Belyavin, K. E. (2004). Poluchenie poristyh materialov iz tugoplavkih metallov metodom elektroimpul'snogo spekaniya. Teoriya i praktika mashinostroeniya, 2, 68–77.
17. Raychenko, A. I., Sizonenko, O. N., Derevyanko, A. V., Kolesnichenko, V. G., Grigor'ev, E. G., Ivliev, A. I. (2012). Osobennosti vozdeystviya elektricheskogo razryada v protsesse konsolidatsii poroshkov. Visnyk NTU «KhPI». Seriya: Tekhnika ta elektrofizyka vysokykh napruh, 52 (958), 146–154.
18. Grigor'ev, E. G. (2008). Kinetika protsessov uplotneniya dispersnyh materialov pri elektroimpul'snom vozdeystvii. Izvestiya RAN. Seriya fizicheskaya, 72 (9), 1210–1212.
19. Ryabinina, O. N. (2006). Tehnologicheskie printsipy vybora materialov press-instrumenta pri elektrorazryadnoy obrabotke metallicheskih poroshkov. Vestnik Orenburgskogo gosudarstvennogo universiteta, 10, 414–421.
20. Raichenko, O. I. (2016). Model of Compaction Process of a Porous Powder Elastic-Viscous Material at Electric Sintering. Metallofizika i noveishie tekhnologii, 38(5), 635–645. doi: https://doi.org/10.15407/mfint.38.05.0635
21. Gevorkyan, E. S., Chishkala, V. A., Kyslytsia, M. V. (2016). Electroconsolidation method (electric sintering) as a highly efficient method for the compaction of nanopowders to obtain composite materials for instrumental and structural purpose. Zbirnyk naukovykh prats UkrDUZT, 160, 75–79.
22. Raychenko, A. I., Sizonenko, O. N., Derevyanko, A. V., Kolesnichenko, V. G., Grigor'ev, E. G. (2012). Analiz izmeneniya sostoyaniya poroshkovyh kompozitsiy pri elektrorazryadnom vozdeystvii (Obzor). Visnyk Ukrainskoho materialoznavchoho tovarystva, 1 (5), 49–56.
23. Zamula, M. V., Derevyanko, A. V., Kolesnichenko, V. G., Samelyuk, A. V., Zgalat-Lozinskiy, O. B., Ragulya, A. V. (2007). Osobennosti elektrorazryadnogo spekaniya nanokompozitov sistemy TiN - AlN. Poroshkovaya metallurgiya, 7–8, 19–27.
24. Morozov, A. (2019). Analysis of the technological and morphological peculiarities of bronzed powders production from the swarf wastes. Technology Audit and Production Reserves, 1 (3 (45)), 24–26. doi: https://doi.org/10.15587/2312-8372.2019.163794
25. Zavaliangos, A., Zhang, J., Krammer, M., Groza, J. R. (2004). Temperature evolution during field activated sintering. Materials Science and Engineering: A, 379 (1-2), 218–228. doi: https://doi.org/10.1016/j.msea.2004.01.052